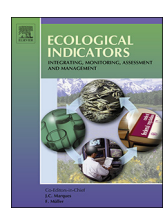
ELSEVIER

Contents lists available at ScienceDirect

Ecological Indicators

journal homepage: www.elsevier.com/locate/ecolind



Quantifying the relationship between streamflow and climate change in a small basin under future scenarios



Hui Wang^{a,*,1}, Scott R. Stephenson^{b,2}, Shijin Qu^{c,3}

- ^a Institute for Modeling Collaboration and Innovation, University of Idaho, Moscow, ID 83844, USA
- b RAND Corporation, Santa Monica, CA 90401, USA
- ^c Department of Land Resources Management, China University of Geosciences, Wuhan, Hubei 430074, PR China

ARTICLE INFO

Keywords: Climate change Hydrology Land use and land cover SWAT Human-environment systems

ABSTRACT

Previous studies have identified the importance of simulating and quantifying the relationship between hydrologic variation and climate change under historical scenarios at regional and continental scales. However, robust demonstration of the potential of combining consistent land use/cover change (LUCC) and climate change to simulate future hydrologic processes is still lacking. Furthermore, investigating the future connections between hydrologic characteristics and climate variables demands exploration of these phenomena at small (basin) scale. To fill this gap, this research simulates land use/cover patterns in 2030 based on the logistic Cellular Automata-Markov model. Then the Soil Water Assessment Tool (SWAT) simulates change in streamflow within the Ashuelot River basin in New England between 2002-2009 and 2032-2039. Projected climate data are obtained from two general circulation models (GCMs) under Representative Concentration Pathways (RCPs) 4.5 and 8.5. We also quantify relationships between the rates of change (RC) of streamflow, precipitation and potential evapotranspiration (PET) among 29 subbasins at a monthly scale between the two time periods under different climate scenarios by implementing a panel data approach. Results show greatest changes in forestland (-21.07 km²) and intensive urban land (+5.4 km²) by 2030. Comparisons between the two periods show a negative overall trend in runoff under RCPs 4.5 and 8.5 for both selected GCMs. Panel data analysis indicates that precipitation may contribute more to the RC of streamflow when change in streamflow is significantly influenced by both PET and precipitation over the study period. Therefore, this study provides an important insight into quantifying and comparing the relationship of basin-scale change between streamflow and future climate.

1. Introduction

Climate change and land cover variability are two major components affecting hydrologic processes (Pfister et al., 2004; Hovenga et al., 2016). These interacting processes involve numerous meteorological and landscape variables such as precipitation, evapotranspiration, solar radiation, temperature, soil type, topography, land use and land cover (Wu et al., 2012). The IPCC AR5 (2014) reports that anthropogenic changes to the global hydrologic cycle will increase spatial and temporal disparities between wet and dry regions. Recent studies found that approximately 36% of the world population experiences water scarcity, especially in developing countries (Von Grebmer et al., 2015). By 2050, 52% of the world's population is projected to be exposed to

severe water scarcity without significant intervention (Wang et al., 2016). In addition to climate variability, land use/cover change (LUCC) caused by human activities also influences hydrologic characteristics such as infiltration, percolation, groundwater and runoff. Specifically, previous research has confirmed that decreasing vegetation and soil infiltration capacity leads to increasing streamflow (Wang and Stephenson, 2018; Zuo et al., 2016; Bronstert et al., 2002).

To better understand these interactions, scientists have investigated the response of hydrologic characteristics to climate change and LUCC by applying various hydrologic models. These models are usually classified as one of three types: empirical, conceptual, and physical (Devia et al., 2015). Although previous studies have shown successful applications of these models in most cases, physically based distributed

^{*} Corresponding author at: University of Idaho, 875 Perimeter Drive, MS 1122, Moscow, ID 83844, USA. E-mail addresses: huiwang@uidaho.edu (H. Wang), sstephen@rand.org (S.R. Stephenson), qusj@cug.edu.cn (S. Qu).

¹ ORCID: 0000-0003-3217-8340.

² ORCID: 0000-0003-4143-2670.

³ ORCID: 0000-0003-0674-568x.

models have outperformed others owing to their ability to represent real physical processes (Jayakrishnan et al., 2005). The Soil and Water Assessment Tool (SWAT), a physically based distributed model, has been widely used to evaluate the impacts of climate change and LUCC on water resources. Implementations of SWAT can be classified into three types based on the variables controlled in each case - climate change, LUCC, and combined climate and LUCC impacts on hydrologic processes. Ouyang et al. (2015) assessed the impact of climate change on streamflow and developed long-term watershed management plans using six global climate models (GCMs). Unival et al. (2015) quantified the impacts of climate change on water balance components in the Upper Baitarani River basin in India by considering several warming scenarios. Can et al. (2015) found that surface runoff declines when forest, agricultural land and grassland increase under different land use scenarios. Yang and Lu (2018) defined two respective land use/cover scenarios for 2000 and 2015 and investigated the effects of the Grainfor-Green Program on runoff and erosion in the Loess Plateau in China. Data preparation in these studies usually includes both climate variables and land use/cover scenarios; however, their approaches to obtaining land use/cover data do not reflect decadal hydrologic variation, particularly when considering long-term climate change.

Recent studies have begun to investigate future climate-driven hydrologic responses using bias-corrected and downscaled GCM outputs and corresponding simulated land use/cover patterns, reflecting the compound effects of climate change and LUCC. However, some uncertainties and limitations remain in those studies due to the lack of a theoretical basis for selecting an optimal method for LUCC simulation. For example, Kundu et al. (2017) used SWAT to quantitatively estimate future water balance in 12 subbasins of the Narmada River basin using a Markov Chain model to generate future land use/cover patterns. Yang et al. (2019) investigated the combined impacts of LUCC and climate change on future runoff in the Luanhe River basin by combining Multi Criteria Evaluation (MCE), cellular automata (CA) and a Markov model. Hipt et al. (2019) used a combination of Multi-Laver Perceptron (MLP) and a Markov model to examine the effect of LUCC and climate change on water resources in a tropical West African catchment. Although these applications show relatively high goodness-of-fit between simulated and reference land use/cover maps, contributions of various driving factors to a specific land use/cover category are missing (Wang et al., 2019), resulting in relatively less convincing predicted hydrologic responses under corresponding future scenarios. Following Wang et al. (2019), these contribution indicators can be reflected by quantitative assessment of relationships between driving factors and land use/cover types; hence we employ an integrated logistic regression-CA-Markov model (LCM) in the present study. This method has been shown to achieve high simulation accuracy of future land use/cover patterns at small scales even when spatial non-stationarity of socio-economic variables is taken into consideration (Wang et al., 2019).

Previous studies have attempted to investigate the relationship between hydrologic variations and climate change using historical records. Xu et al. (2011) found that periodic changes in runoff, temperature and precipitation are closely correlated, and they found a significant and positive correlation of these variables with annual runoff at different temporal scales. Wang et al. (2017) quantified the relationship between runoff indices (i.e., maximum daily discharge difference and accumulated direct discharge), precipitation and temperature by applying a multiple linear regression method. Moreover, Duan et al. (2017) showed that temperature plays a more important role than precipitation in variation of runoff during the late-21st-century under global warming, although precipitation has played a more important role in the last several decades. Their results suggest that the contribution of temperature to hydrologic change has been underestimated under future climate and LUCC scenarios in the conterminous United States. In addition, scientists believe that temperature and precipitation will continue to influence the magnitude and fluctuation of hydrologic characteristics, such as streamflow, throughout the 21st century (McCabe and Wolock, 2011; Wu et al., 2018). Other climate variables such as potential evapotranspiration (PET) also impact water resources through indirect effects from temperature, solar radiation and wind (Wang and Stephenson, 2018). Thus, further research on the dynamic influence of these climate variables under plausible future climate scenarios is needed. Although studies on these relationships are relatively well-developed at regional and continental scales, details of their connections within small basins and among their adjacent subbasins remain lacking.

Evidence that runoff in small basins is more sensitive to the spatial distribution of precipitation has been demonstrated previously (Biemans et al., 2009), such that small differences in climate variables (e.g., precipitation) between adjacent subbasins of a small basin may result in large differences in runoff. However, few studies have attempted to use these small differences to investigate the correlation between hydrologic characteristics, precipitation and temperature. Therefore, it is necessary to take these differences into consideration when reexamining the correlation between hydrologic and climate factors within a small basin, especially under future climate scenarios. Moreover, most previous research at a given spatial scale derived such correlations based only on an average value applied to an entire area, neglecting the potential non-stationarity of both dependent and independent variables among subbasins. Therefore, under these conditions, the time periods, adjacent subbasins, and hydrologic and climate variables comprise a multi-dimensional dataset often recognized in the field of econometrics as panel data. Previous research demonstrated that panel data may be better than cross-sectional data in analyzing the dynamics of variation, such as the transition behavior of resource utilization (Fan et al., 2017). This study will therefore apply panel data to investigate the quantitative relationship between change in streamflow and climate change within a small basin under future climate scenarios.

As a whole, this study mainly focuses on simulating change in streamflow within a small basin under future LUCC and climate scenarios by integrating LCM and the SWAT model. After obtaining future simulated data for each subbasin within a small basin, the rate of change (RC) of streamflow can be calculated between selected historical and future time periods. The research then aims to quantitatively assess the relationship of RC between streamflow and climate variables (e.g., precipitation and PET) in the future. Specifically, this study will address the following research questions: (1) How will streamflow change under varying warming scenarios projected by different GCMs when a corresponding optimal future LUCC scenario is applied? (2) How can we characterize the diversity of change in streamflow among subbasins within a small basin? (3) What is the correlation of RC between streamflow and climate variables among subbasins within a small basin?

2. Study area and data

2.1. Selection of study area

We select the Ashuelot River basin, a part of the Connecticut River basin in the Northeastern United States, as our study area (Fig. 1). The US Northeast has experienced the strongest regional extreme precipitation increase in the United States in the last 50 years (Parr and Wang, 2014). The Ashuelot River originates from Pillsbury State Park in Washington, New Hampshire and flows 103 km before discharging into the Connecticut River in Hinsdale, New Hampshire. The basin encompasses approximately 1100 square kilometers and covers 27 towns in southwestern New Hampshire and Massachusetts. The river has attracted increasing attention since 1991 when the Silvio O. Conte National Fish and Wildlife Refuge Act was passed to protect and improve the diversity of species in the Connecticut River basin (Zimmerman and Lester, 2006). According to the 2006 Ashuelot River Corridor Management Plan (Skuly et al., 2006), frequency of flooding events is increasing along the river bank due to expanding impervious land in the

H. Wang, et al.

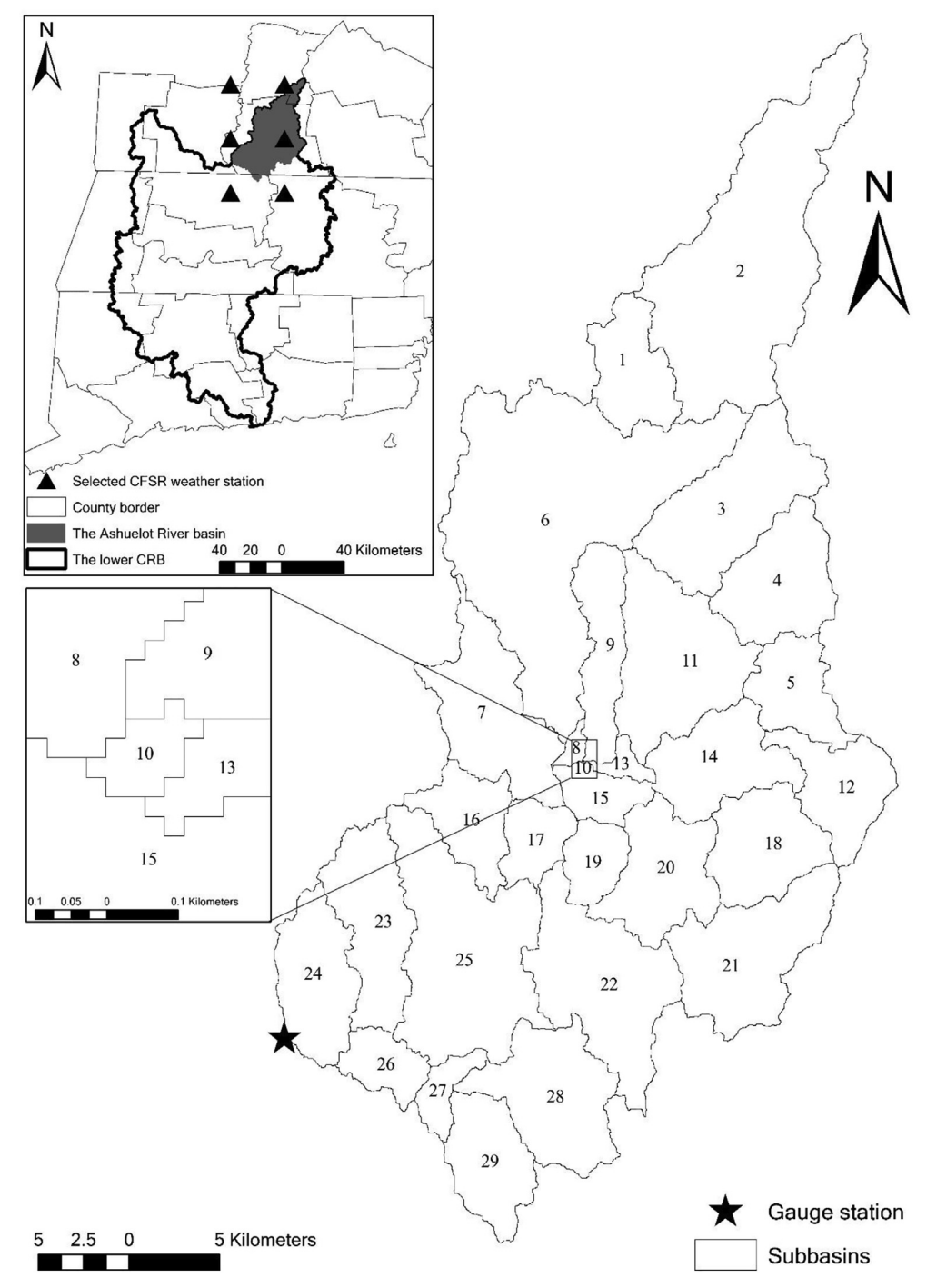


Fig. 1. Location of the Ashuelot River basin and numbered subbasins (main map) and lower Connecticut River Basin (inset map).

basin. Moreover, ecological changes, such as forest loss and shift, are projected to become more severe by late-century under a high greenhouse gas scenario (Sintros et al., 2010).

The Ashuelot River basin plays an ecologically and culturally significant role in southwest New Hampshire, providing wildlife habitat and recreational resources. A land conservation plan for the basin published by the Nature Conservancy, the Monadnock Conservancy, the Society for the Protection of New Hampshire Forests, and the Southwest Region Planning Commission highlights pressures in the region caused by an expansion of new roads, sprawling development and some irreversible LUCC (Zankel, 2004). Moreover, the 2010 Sustainability Project for Forest and Water Climate Adaptation also projected increasing loss of forest due to urban development in the next several decades,

raising the likelihood of extreme streamflow events. As these concerns are common to many river basins throughout the northeast, it is appropriate to regard the Ashuelot River basin as a typical small basin in our study region.

2.2. Data acquisition and management

We obtained slope and elevation data from the National Elevation Dataset digital elevation model (DEM) to delineate boundaries of the basin and its subbasins. Three periods of 30-meter spatial resolution land use/cover maps (2001, 2006 and 2011) were acquired from the National Land Cover Database (NLCD). For compiling with the land use/cover classification system of SWAT, we reclassified the NLCD data

Table 1Reclassification of land use/cover type.

SWAT land use/ cover type	NLCD classification	Description
WATR	Open water, woody wetlands, emergent herbaceous wetlands	Water
URBN	Developed area	Intensive urban land
PAST	Barren land, grassland, pasture	Pasture
FRSD	Deciduous forest, evergreen forest, mixed forest	Forestland
RNGB	Shrub	Shrubland
AGRL	Cultivated crops	Agricultural land

into six land use/cover types (Table 1). Soil data were downloaded at a scale of 1:24000 from the Soil Survey Geographic Database (SSURGO) maintained by the US Department of Agriculture (USDA) Natural Resources Conservation Service (NRCS). Six independent variables covering both physical and socio-economic attributes for LCM were selected following Wang et al. (2019). In addition to slope and elevation data obtained for SWAT inputs, distance to main roads and distance to town centers in 2010 from US Census Bureau TIGER datasets were chosen as proximity variables to show the impacts of location on land use/cover simulation processes. In addition, socio-economic factors, specifically population density and per capita income in 2010, were acquired from the U.S. Geological Survey (USGS) and US Census Bureau TIGER datasets, respectively.

Due to limited real-time weather stations in our study basin, historical meteorological data (daily precipitation, daily maximum and minimum temperature, average daily relative humidity, average daily wind speed and daily solar radiation) from 1979 to 2013 were obtained from the Climate Forecast System Reanalysis (CFSR) global meteorological dataset as SWAT inputs. Fuka et al. (2014) demonstrated that the CFSR data perform as well as or better than traditional meteorological gauging data in simulating streamflow. These data provide an alternative to in-situ meteorological data where such data are insufficient to represent historical weather records. Average monthly PET calculation follows the Penman-Monteith equation (Allen et al., 1998). Fig. 1 shows the spatial distribution of six CFSR meteorological stations in the study area. Future hydrologic simulation from 2030 to 2039 is driven by outputs from two general circulation models (GCMs) (bcccsm1-1 and HadGEM2-CC) under two Representative Concentration Pathways (RCP 4.5 and RCP 8.5). The bcc-csm1-1 is developed by the Beijing Climate Center and is a fully coupled, relatively low-resolution $(2.8^{\circ} \times 2.8^{\circ})$ climate system model incorporating the global carbon cycle and dynamic vegetation cover (Wu et al., 2014). The HadGEM2-CC, developed by the Met Office Hadley Centre, belongs to the Hadley Centre Global Environmental Model version 2 (HadGEM2) family. This model includes various Earth system components such as troposphere, land surface and hydrology, and terrestrial carbon cycle while omitting tropospheric chemistry, with a moderate resolution (1.88°×1.25°) (Bellouin et al., 2011). High-resolution (4 km) gridded climate outputs for these models were downloaded from the Multivariate Adaptive Constructed Analogs (MACA) dataset, which uses statistical downscaling to remove biases from raw GCM outputs (Abatzoglou and Brown, 2012). A recent study by Karmalkar et al. (2019) evaluated the 36 GCMs in the northeastern U.S., showing that bcc-csm1-1 (hereafter, "bcc") and HadGEM2-CC (hereafter, "Hadley") rank #2 and #16, respectively, based on selected performance metrics. Moreover, due to data accessibility and wide applicability, these models were selected to represent a range of variability in hydrologic simulations. Corresponding historical monthly discharge data from 1981 to 2013 for calibration and validation were acquired from the USGS Water Data for the Nation (USGS Water Resources).

3. Methodology

3.1. Modeling workflow

To understand the relationships of RC between streamflow, precipitation and PET under future scenarios, our methodology comprises three modules: 1) calibration and validation of LCM and simulation of future land use/cover patterns; 2) calibration and validation of SWAT model and simulation of future change of streamflow under RCP 4.5 and RCP 8.5 of two selected GCMs; 3) eligibility examination (i.e., unit root test and cointegration test) and utilization of a linear regression model for the panel dataset. Descriptions of each module are given below.

3.2. Simulation of LUCC by LCM

Creating suitability maps of various land use/cover categories is an important component of LUCC forecasting. Unlike subjective scoring methods such as MCE, logistic regression is able to robustly evaluate quantitative relationships between driving factors and land use/cover categories based on socio-economic and physical variables (Arsanjani et al., 2013). Therefore, the suitability of a specific land use/cover category in each grid cell can be expressed as a function of the values of selected independent variables. Coefficients derived from the regression model are applied to the entire study area, representing the contribution of corresponding driving factors to a land use/cover category. Although previous research has incorporated the spatial non-stationarity of independent variables in logistic regression for simulating LUCC with an integrated CA-Markov model approach, the sensitivity of simulated LUCC to spatial non-stationarity was found to be low for a subbasinscale study area within the Connecticut River basin (Wang et al., 2019). Moreover, LUCC maps simulated by LCM also achieve high agreement with observed data. Therefore, the present study mainly focuses on employing logistic regression to create suitability maps, and then to generate future land use/cover patterns as initial inputs to the SWAT model.

Integrated CA-Markov model has been widely used in LUCC analysis in recent years (Iacono et al., 2015; Subedi et al., 2013; Halmy et al., 2015). This combined approach simulates LUCC through both spatial and temporal transitions of land use/cover categories over a given period. Over predefined rounds of iteration, CA model predicts the following status of each pixel based on its current status, its neighboring impacts, and a predefined transition rule. Specific predefined rounds of iteration determine whether each pixel changes or remains unchanged. This process follows the rule that pixels will be more likely to change to a certain land use/cover category when the transition probability for that category is high (Wu, 2002).

While the CA model is capable of simulating the spatial interactions between neighborhoods, the Markov model aims to provide the number and probability of pixel transitions between two adjacent time steps (Sang et al., 2011). The modeling process is stochastic, and the next status of each pixel at time t+1 only depends on its status at time t by applying the transition probability matrix. The transition probability matrix and Markov process can be expressed as follows:

$$P_{ij} = \begin{bmatrix} p_{11} & \cdots & p_{1n} \\ \vdots & \ddots & \vdots \\ p_{n1} & \cdots & p_{nn} \end{bmatrix} (\sum_{j=1}^{n} p_{ij} = 1, (i, j = 1, 2 \cdots, n)$$
(1)

$$P_{ij} \times D_t = D_{t+1} \tag{2}$$

where P_{ij} is the transition probability matrix for the selected land use/cover categories over two time stages; n represents the total number of land use/cover categories; and D_t and D_{t+1} denote the land use/cover category proportion vector for time t and t+1, respectively.

Based on this framework, we first simulate the 2011 land use/cover pattern based on the 2001 and 2006 land use/cover map. This process

involves generating the suitability map for each land use/cover category in 2006 by utilizing a logistic regression model and establishing transition rules (e.g., transition probability matrix from Markov model) for simulation. The 2011 ground-truth land use/cover map is treated as reference data for evaluating the accuracy of simulation results. Three Kappa indices, specifically traditional Kappa ($K_{standard}$), Kappa for no ability (K_{no}) and Kappa for location ($K_{location}$), are employed in this validation process. Lastly, the land use/cover maps of 2001 and 2006 are used to simulate 2030 land use/cover if the aforementioned Kappa indices demonstrate substantial agreement (0.61–0.80) or almost perfect agreement (> 0.80) (Viera and Garrett, 2005).

3.3. SWAT model simulation

The SWAT model is a physically-based and semi-distributed hydrologic model developed by the U.S. Department of Agriculture (USDA) Agricultural Research Service (ARS) (Gassman et al., 2007). It has been widely used to investigate the impacts of climate change and LUCC on water resource quantity and quality at various scales (Arnold et al., 1998; Gassman et al., 2007). Within the SWAT model framework, a basin is delineated and can be divided into subbasins based on a DEM. It is then further divided into Hydrologic Response Units (HRUs) representing basic simulation traits, encompassing a single soil type, land use/cover category and range of slope. Hydrologic components, such as evapotranspiration, streamflow and percolation, are simulated from these smallest parcel units to the subbasin level, and accumulated at the outlet through the entire stream network. Consequently, the daily water budget may be calculated in an individual basin. The SWAT model follows a water balance equation to simulate hydrologic components. The equation can be expressed as:

$$SW_t = SW_0 + \sum_{t=1}^{t} (R_d - SURQ_d - ET_d - PERC_d - QR_d)$$
(3)

where SW_t is the soil water content at the end of the study period; SW_0 is the soil water content at the beginning of the study period; R_d is daily precipitation during the time period t; $SURQ_d$ is daily surface runoff; ET_d is amount of daily evapotranspiration; $PERC_d$ is daily percolation and QR_d represents the daily amount of return flow (Arnold et al., 1998). The unit in this equation is mm.

Before simulating the historical and future streamflow utilizing SWAT, calibration and validation must be performed by comparing simulated streamflow data with the corresponding observed streamflow data obtained from the same gauge station over a given time period. Moreover, previous studies demonstrated that not all hydrologic parameters accounted for in SWAT may significantly affect the simulated results (Cibin et al., 2010). SWAT Calibration and Uncertainty Programs (SWAT-CUP) enables sensitivity analysis of parameters, calibration, validation, and uncertainty analysis of SWAT model results (Abbaspour, 2013). The Sequence Uncertainty Fitting algorithm (SUFI-2) is selected to optimize parameters due to its ability to consider uncertainties from various sources, such as driving factors, observed data, and the conceptual model specification (Abbaspour, 2013). Significance of parameters in model calibration is assessed by a two-tailed t-test in SWAT-CUP. Parameters are more sensitive when the absolute value of the t statistic is large (statistical significance at p < .05). In the present study, model performance is evaluated by three indicators: coefficient of determination (R^2), the Nash-Sutcliffe coefficient (E_{NS}) and percent bias (PBIAS). The equations of these indicators are expressed as follows:

$$R^{2} = \left[\sum_{a=1}^{b} (Q_{o,a} - \bar{Q_{o}})(Q_{s,a} - \bar{Q_{s}}) \right]^{2} / \sum_{a=1}^{b} (Q_{o,a} - \bar{Q_{o}})^{2} \sum_{a=1}^{b} (Q_{s,a} - \bar{Q_{s}})^{2}$$

$$(4)$$

$$E_{NS} = 1 - \sum_{a=1}^{b} (Q_o - Q_s)_a^2 / \sum_{a=1}^{b} (Q_{o,a} - \bar{Q_o})^2$$
(5)

PBIAS =
$$100 * \sum_{a=1}^{b} (Q_o - Q_s)_a / \sum_{a=1}^{b} Q_o$$
 (6)

where Q_o represents the observed streamflow data; Q_s represents the simulated streamflow data from SWAT; \bar{Q}_o is the average of the observed data; \bar{Q}_s is the average of the simulated data; b is the number of records; and a is the a^{th} observed or simulated streamflow data.

Based on the topographic attributes of the Ashuelot River basin, this research divides the study area into 29 subbasins. The SWAT model is calibrated for the period from 1981 to 1996, and validated for the period from 1997 to 2013, ensuring an optimal balance of time period. In addition, 1979 and 1980 are treated as warm-up years for initialization the model. The 2001 land use/cover map is used for delineation of the HRUs and calibration and validation of the model.

3.4. Panel data analysis

Over the last several decades, panel data analysis has been widely used in analyzing the impacts of environmental phenomena on human systems, such as identifying and quantifying impacts of climate change and extreme weather events on agricultural yields (Naudé, 2004; Aşıcı, 2013; Powell and Reinhard, 2016; Massetti and Mendelsohn, 2011). The more common time series and cross-sectional data may be considered simplified forms and special cases of panel data: time series data may span a long time period but usually encompass a single area, while cross-sectional data cover many areas at a single point in time. However, panel data can include measurements of multiple variables over selected time periods for each subbasin within a large basin (Fitzmaurice et al., 2012). In this research, our panel data consist of 29 subbasins from January to December for two study periods. Independent variables include the RCs of streamflow, precipitation and PET between Period 1 (2002–2009) and Period 2 (2032–2039).

Before employing least squares regression with panel data, the reliability and applicability of input variables and the stability of the relationship between dependent and explanatory variables across the dataset must be investigated (Levin et al., 2002; Kao, 1999). Specifically, we examine the stationarity of dependent and independent variables over each period to avoid spurious regression using a unit root test. In order to mitigate uncertainties stemming from reliance on one test, four tests (Levin-Lin-Chu [LLC] t test, Im-Pesaran-Shin [IPS] w test, Fisher-ADF [F-ADF] test, and Fisher-PP [F-PP] test) are performed. After passing the unit root test, a cointegration test is applied to ensure the stationary relationship between dependent and independent variables. Following Pedroni (1999) and Kao (1999), we employ a Pedroni test (i.e., Panel/Group ADF, Panel/Group PP) and Kao test to assess the existence of cointegration. Fixed-effects regression, rather than randomeffects regression, was selected owing to the relatively small number of subbasins (29) and their similar effect sizes (Borenstein et al., 2010).

4. Results and discussion

4.1. Simulation of future LUCC by LCM

Based on the observed 2001 and 2006 land use/cover maps, a Markov transition matrix of land use/cover categories between 2001 and 2006 is generated. On the basis of the observed 2006 land use/cover pattern and the raster maps of six selected independent variables, suitability maps for six land use/cover categories (WATR, URBN, PAST, FRSD, RNGB and AGRL) are obtained using a logistic regression model. We then simulate 2011 land use/cover for validation by integrating the Markov transition matrix, suitability maps and predefined CA transition rules in a CA-Markov model. Fig. 2(3) and Fig. 2(4) show the observed and simulated 2011 land use/cover maps, respectively. Visual comparisons between these maps illustrate that most simulated areas exhibit high agreement with the observed data. Three Kappa indices employed to validate the accuracy of the LCM model indicate that the

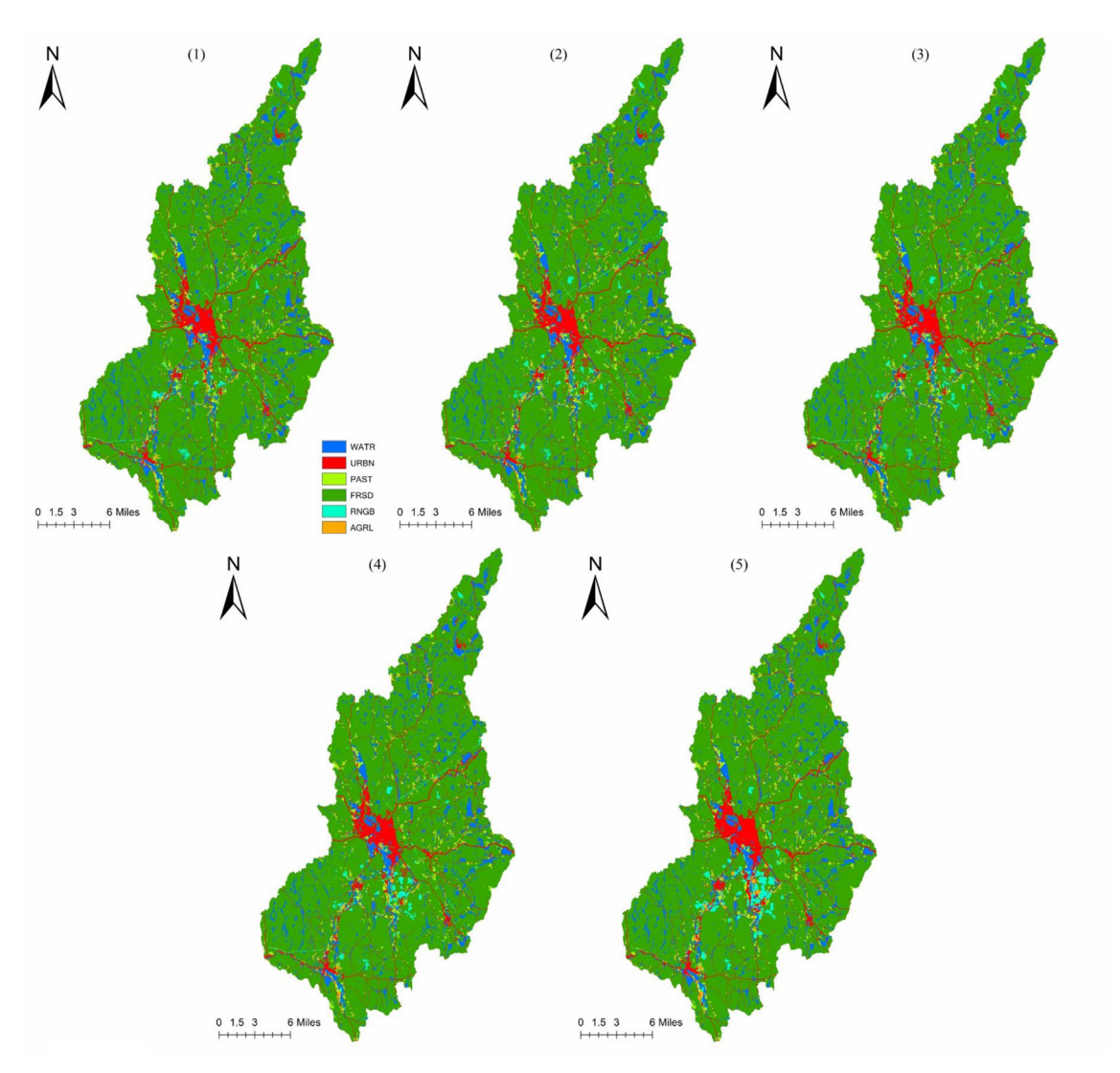


Fig. 2. Land use/cover maps of (1) observed 2001, (2) observed 2006, (3) observed 2011, (4) simulated 2011, and (5) simulated 2030 data.

Table 2
RC and area of land use/cover transitions between 2001, 2011 and 2030.

Land use/cover type	2001	2001–2011	2001–2011			2001–2030		
		Gain	Loss	Net change	Gain	Loss	Net change	
WATR	89.63	0.05 (0.06)	0.31 (0.34)	-0.26	0.16 (0.18)	1.37 (1.53)	-1.21	
URBN	70.58	1.31 (1.85)	0 (0)	1.31	5.40 (7.65)	0 (0)	5.40	
PAST	33.16	1.49 (4.5)	1.24 (3.74)	0.25	4.30 (12.98)	5.17 (15.60)	-0.87	
FRSD	874.13	1.05 (0.12)	7.43 (0.85)	-6.38	4.02 (0.46)	21.07 (2.41)	-17.05	
RNGB	10.19	3.95 (38.72)	1.17 (11.47)	2.78	7.23 (70.96)	4.05 (39.78)	3.18	
AGRL	2.60	0.43 (16.61)	0.05 (2.11)	0.38	1.37 (52.74)	0.23 (8.92)	1.14	

Note: Values in bracket denote RC %. Values out of bracket denote area with the unit of km^2 .

simulated 2011 land use/cover map exhibits almost perfect agreement with the observed data, with $K_{standard}$ of 97.05%, K_{no} of 98.79% and $K_{location}$ of 97.29% (Viera and Garrett, 2005). These values underscore the validity of the LCM model and suggest confidence in its ability to simulate future LUCC in our study area with high accuracy. Table 2 shows the area of each land use/cover category in 2001 and rates of change of land use/cover transitions between 2001 and 2011. In 2001, forestland occupied the largest area in the Ashuelot River basin (approximately 81%). However, from 2001 to 2011, forestland also had the largest net change area (6.38 km^2) compared with the other land use/cover categories, with a gain of $1.05 \ km^2$ and loss of $7.43 \ km^2$. This

result aligns with the finding of the 2010 Sustainability Project that forest area declined significantly from 2000 to 2010. Table 2 also shows that shrubland experienced the largest area increased $(3.95\ km^2)$ in these ten years. More interestingly, results even indicate that intensive urban land area increased by 1.85% (1.31 km^2), with no decrease during this time period.

Following the Markov transition matrix obtained in the previous step, LUCC in 2030 is simulated based on the observed 2006 land use/cover map and the 2006 suitability map of each land use/cover category (Fig. 2(5)). Table 2 also shows the degree of land use/cover transition between 2001 and 2030. Variation trends of land use/cover

Table 3Selected SWAT parameters.

Parameters	Range	Description
V_CH_N2	0–1	Manning coefficient for main channel
V_SFTMP	- 5-5	Snowfall temperature (oC)
V_ALPHA_BNK	0-1	Baseflow alpha factor for bank storage
V_CANMX	0-95	Maximum canopy storage
R_SOL_K	-1.5-1.5	Soil conductivity (mm/h)
V_CH_K2	0-150	Hydraulic conductivity in main channel (mm/h)
V_EPCO	0-1	Plant evaporation compensation factor
R_CN2	-0.7-0.7	Soil conservation service runoff curve number for
		moisture condition II

Note: V_{\perp} means the existing parameter value is to be replaced by a given value. R_{\perp} means the existing parameter value is multiplied by (1 + a given value).

categories over this period are similar to those from 2001 to 2011. Across the entire Ashuelot River basin, forestland is again projected to exhibit the greatest decrease (21.07 km^2) during this period. Although shrubland gains 70.96% of its area (7.23 km^2) by 2030, almost 40% of its area (4.05 km^2) will be converted during the same period. Therefore, this leads to a net increase of 3.18 km^2 for shrubland in the study area. Urban area also increases in the next decade, with an increasing rate of 7.65%. Our findings are in agreement with those of Thorn et al. (2017) that impervious cover is projected to increase in southern New Hampshire in the future.

4.2. Simulation of future streamflow by SWAT model

During the calibration process, sensitivity of parameters is investigated and parameters are adjusted to achieve optimal model outputs. Table 3 shows the 8 parameters considered to be the most sensitive to the estimation of streamflow in this study (Kundu et al., 2017; Yang et al., 2019). The performance of the calibrated SWAT model is evaluated by three indicators (i.e., R^2 , E_{NS} and PBIAS). Following the conclusions of Moriasi et al. (2007) and Almeida et al. (2018), the SWAT model exhibits satisfactory performance when $0.50 < R^2 \le 0.60$, $0.36 < E_{NS} \le 0.60$ and $\pm 15 < PBIAS \le \pm 25$. For calibration of monthly streamflow, R^2 , E_{NS} and PBIAS are 0.74, 0.68 and 2.8, respectively. Validation of monthly streamflow shows that R^2 , E_{NS} and PBIAS are 0.66, 0.47 and -22.9, respectively. Therefore, both calibration and validation demonstrate satisfactory agreement between observed and simulated streamflow, indicating that the calibrated SWAT model is applicable for simulating hydrologic processes in the study area (Fig. 3).

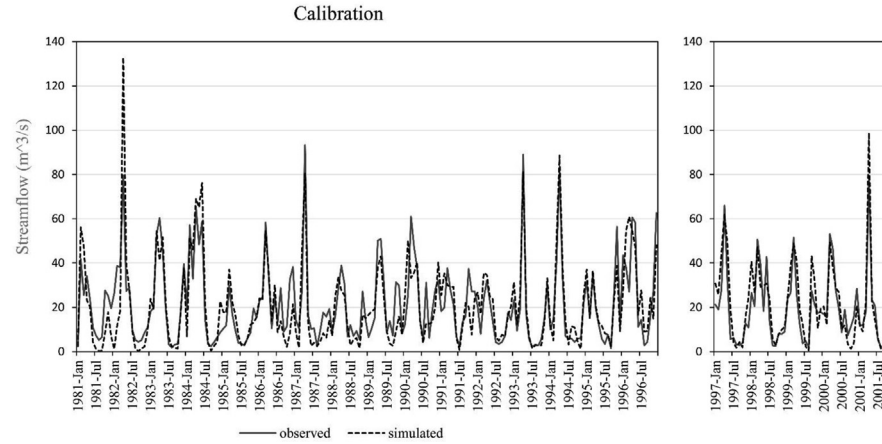
After integrating the simulated 2030 land use/cover map with downscaled GCM outputs, streamflow data in Period 2 (2032–2039) are projected by applying the calibrated SWAT model. To avoid unequal conditions of accumulation and the impact of basin size on

comparability, we use surface runoff to assess the differences between subbasins under both historical and future scenarios (Langbein, 1949). Fig. 4 shows comparisons between monthly observed runoff in Period 1 and simulated runoff in Period 2 for the 29 subbasins. Specifically, Fig. 4A shows that annual peak runoff in Period 2 is projected to be lower than that of Period 1 for each subbasin under RCP 4.5. Fig. 4B illustrates a similar finding under RCP 8.5, indicating that peak runoff that usually occurs in March and April will decrease substantially under future climate change. Fig. 5 shows the average monthly runoff of all subbasins for Period 1 and different scenarios of Period 2. Compared with Period 1, runoff is lower under both GCMs and climate scenarios from 2032 to 2039. Furthermore, both GCMs project smaller average monthly runoff under RCP 8.5 than RCP 4.5, underscoring the potential threat to water resources from a high greenhouse gas emissions scenario. However, our previous finding that the study area will experience decreasing forest area and increasing urban area (section 4.1) suggests that runoff may increase in the future if only LUCC is taken into consideration. Therefore, we conclude that future runoff variations may be influenced more by climate change than LUCC in our study area, with larger decreases in runoff under higher warming scenarios (RCP 8.5).

Monthly RC of streamflow for all 29 subbasins illustrates how streamflow during Period 2 changes relative to that of Period 1, where positive and negative RCs refer to increasing and decreasing streamflow, respectively. Fig. 6 shows the scatter plots (348 points) of RC of streamflow between Period 1 and Period 2 under RCP 4.5 and RCP 8.5 while examining the Hadley and bcc GCMs separately. It also further depicts the close alignment of the RCs under RCP 4.5 and RCP 8.5 for a given model. Results clearly indicate that the streamflow RCs in the bcc model have a better linear correlation than in the Hadley model. In other words, the linearity of impact of two RCP scenarios on future change of streamflow is relatively stronger in the bcc model and weaker in the Hadley model. Moreover, densely clustered points in the third quadrant of Fig. 6b clearly show that the negative RC of streamflow projected by the bcc model is dominant under both RCP 4.5 and RCP 8.5. Although the cluster of points in Fig. 6a is less dense than that in Fig. 6b, the largest number of points fall in the third quadrant (approximately 42% overall). This finding indicates that the tendency of variation of streamflow is decreasing monthly when both climate models are examined.

4.3. Relationship analysis of RC

As mentioned above, panel unit root and cointegration tests are required before applying a least squares regression model. Table 4 shows the estimates of three panel unit root tests, including the significance level of each variable under two RCPs. The results indicate



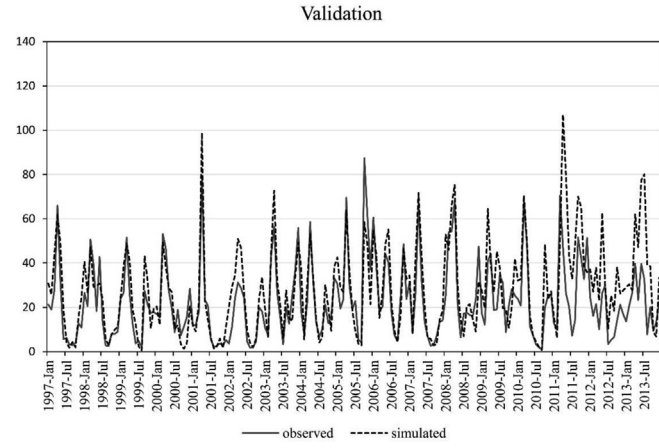


Fig. 3. Observed and simulated monthly streamflow at the #24 subbasin gauge station for calibration (1981–1996) and validation (1997–2013).

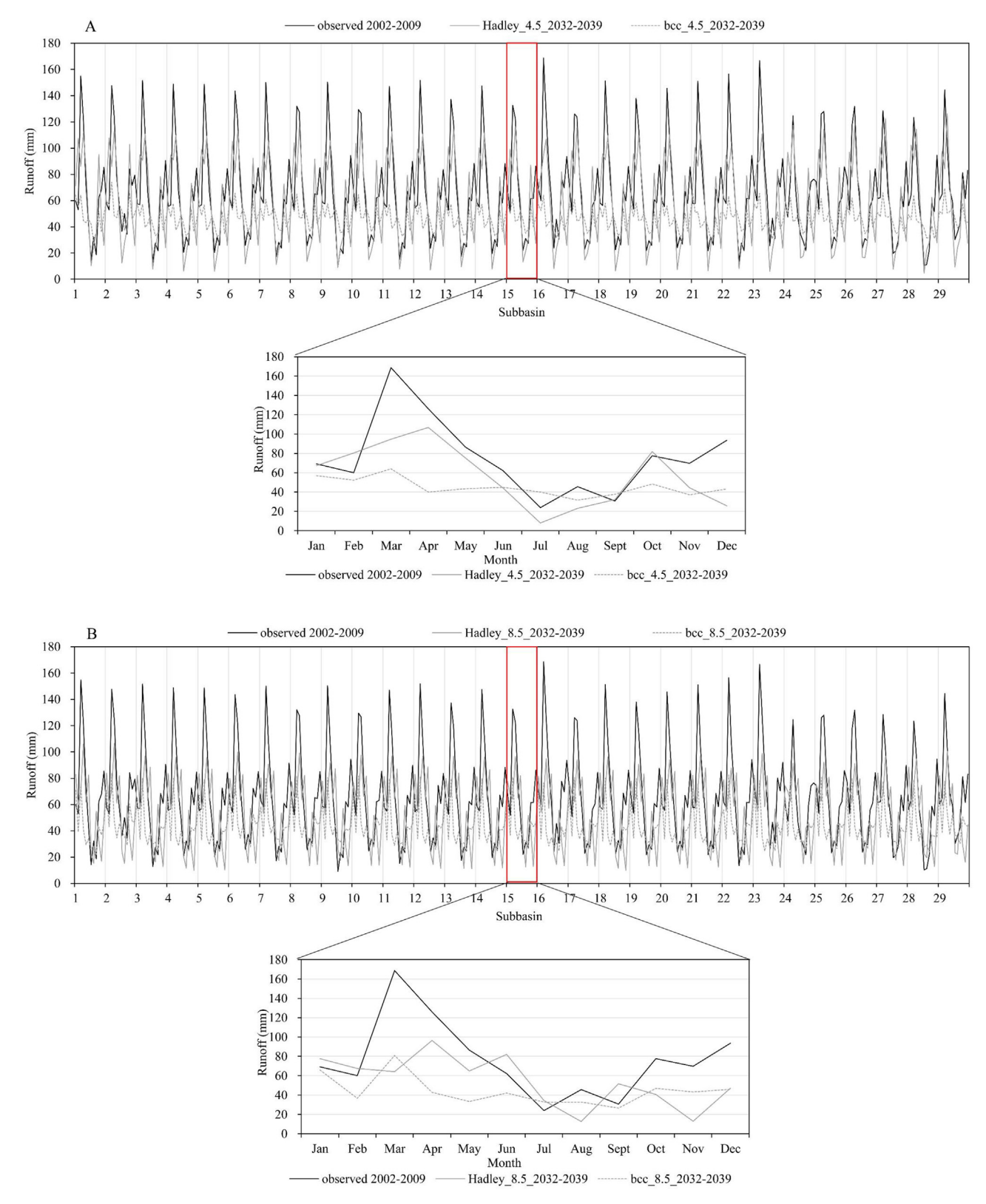


Fig. 4. Comparisons between observed runoff of Period 1 (2002–2009) and simulated runoff of Period 2 (2032–2039) at monthly level for 29 subbasins (subplot A: RCP 4.5; subplot B: RCP 8.5).

that the RCs of streamflow, precipitation and PET are stationary over the time series. Moreover, the null hypothesis that variable non-stationarity exists over the time series can be rejected mainly at the 1% significance level. These findings suggest the absence of spurious regression, and it is therefore reasonable to proceed with a cointegration test using the same variables. Table 5 shows the results of the cointegration test between the RC of streamflow and two independent variables. For both RCPs for each GCM, both the Pedroni test and Kao test reject the null hypothesis at either the 5% or 1% significance level, suggesting a long-term cointegration relationship between the

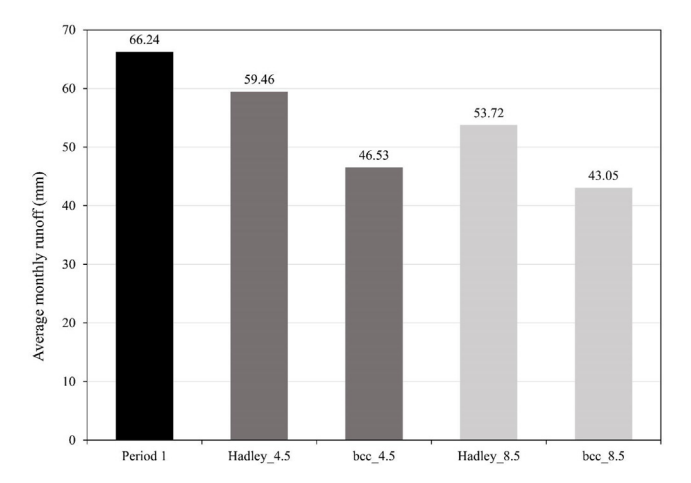


Fig. 5. Average monthly runoff of 29 subbasins for Period 1 and two RCPs of Period 2.

dependent and independent variables. Based on these conclusions, we proceed with quantifying the relationship of RC between streamflow and climate variables through regression analysis.

In regression analysis, positive and negative RCs represent increasing and decreasing variables of the latter period, respectively. In the present study area covering the states of Massachusetts and New Hampshire, an increasing PET leads to decreasing streamflow as actual evapotranspiration is close to PET in this region (Golubev et al., 2001). Therefore, in Table 6, a negative correlation between the RC of streamflow (DF) and the RC of precipitation (DPET) is expected if the variable of the RC of precipitation (DPRP) remains constant.

Several conclusions can be drawn based on Table 6. For the bcc model, coefficients of DPRP and DPET are all significant at either the 1% or 5% level, indicating that the RCs of these two climate variables are closely associated with that of streamflow between Period 1 and Period 2. As expected, DPRP and DPET represent positive and negative contributions to DF, respectively. Moreover, it is clear that the impact of DPET on DF is relatively smaller than that of DPRP on DF, suggesting that variation of precipitation may play a much more important role than that of PET in change of streamflow during the 2030s in the Ashuelot River basin. However, the Hadley model presents a different story. Under RCP 8.5, although the coefficient of DPRP is significant at the 1% level, DPET is not significantly correlated with DF, revealing that the impact of PET on streamflow variation during this period may be minor. However, under RCP 4.5, both DPRP and DPET have significant positive correlations with DF, contrasting with the results of DPET under RCP 8.5 and the expectation of negative correlation between DF and DPET. These contrary findings are probably due to overestimation of positive DPRP caused by high precipitation under this scenario in the Hadley model. Fig. 7 illustrates the distribution of DPRP

and its corresponding DF under RCP 4.5 for both GCMs. It clearly shows greater correlation of positive DPRP and DF in the Hadley model (i.e., first quadrant of Fig. 7a) than in the bcc model (Fig. 7b), suggesting that positive DF is exaggerated due to overestimation of DPRP in the Hadley model. This conclusion is supported by both Hanson (1991) and Fekete et al. (2004). They found that any estimated error in precipitation can translate to streamflow error in wet regions, such as New England. Therefore, it is reasonable that the positive correlation between DF and DPET in this case may be caused by overestimation of positive DF and a positive DPET influenced by warming temperature. Furthermore, this evidence supports the conclusion of Karmalkar et al. (2019) that the bcc model demonstrates greater skill than the Hadley model in the northeastern U.S. region.

5. Conclusion

This research quantifies the relationship of RC between streamflow and two climate variables (precipitation and PET) in the Ashuelot River basin under future climate change and LUCC scenarios. We present three main conclusions. First, we simulate the land use/cover map of 2030 with high accuracy using an integrated LCM model. Forestland is projected to convert the largest area (-21.07 km^2) among all land use/ cover categories by 2030, while urban area will continue to increase in next decade ($+5.4 \text{ km}^2$). Second, historical (Period 1: 2002–2009) and future (Period 2: 2032-2039) streamflow data for all 29 subbasins are simulated using a calibrated SWAT model and downscaled outputs from two GCMs under two warming scenarios. Comparisons between Period 1 and Period 2 show overall decreasing runoff under RCP 4.5 and RCP 8.5 in both bcc and Hadley models. We also expect that warmer temperatures and higher greenhouse gas emissions may result in continued decreasing runoff in the future (Fig. 4). Lastly, panel data analysis is applied to investigate the relationship of RCs between streamflow, precipitation and PET under future climate scenarios. Results of regression analysis indicate that the RCs of precipitation and PET are significantly related to that of streamflow in the bcc model over the study periods. At the same time, the RC of streamflow is influenced more by the RC of precipitation rather than that of PET. Additionally, results from the Hadley model are strongly influenced by its overestimated positive RC for precipitation, resulting in an overestimation of positive RC of streamflow. With the positive RC of PET caused by warming temperatures, the exaggerated positive RC of streamflow consequently leads to a positive correlation between these two variables, contrary to our expectations. We therefore conclude that the bcc model is more reliable in our study area.

Although this study provides an important insight into understanding the future quantitative relationship between streamflow and climate in a small basin, some limitations remain in the modeling process leading to some uncertainty in the results. Due to limited availability of data on socio-economic factors and biophysical land-scapes, we are unable to simulate LUCC that corresponds exactly with

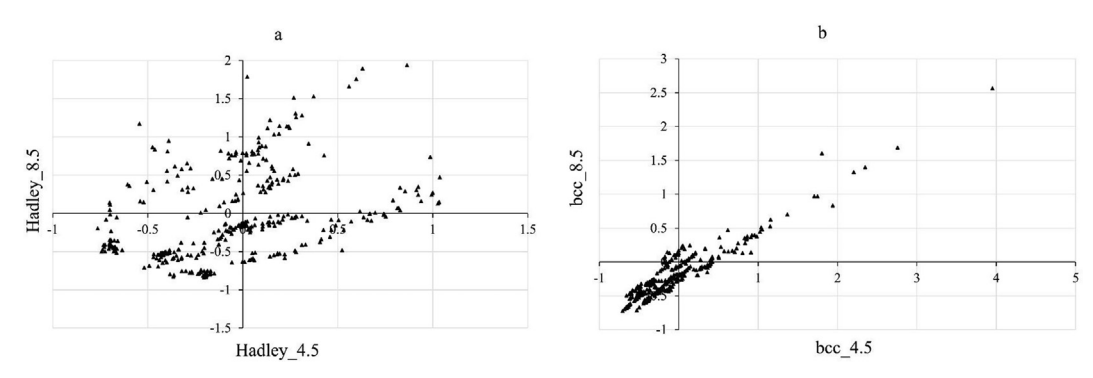


Fig. 6. Scatter plots of monthly RC of streamflow between Period 1 and Period 2 for 29 subbasins under RCP 4.5 and RCP 8.5 of the Hadley model (a) and bcc model (b). Quadrant numbering proceeds counter-clockwise from the upper right.

Table 4
Panel unit root test statistics.

Test type	Scenario	DF	DPRP	DPET
LLC test (bcc)	RCP 4.5	-1.68 (0.046)**	-13.87 (0.000)***	-10.88 (0.000)***
	RCP 8.5	-3.57 (0.000)***	-26.54 (0.000)***	-12.86 (0.000)***
IPS test (bcc)	RCP 4.5	-2.63 (0.004)***	-10.39 (0.000)***	-6.10 (0.000)***
	RCP 8.5	-3.46 (0.000)***	-18.42 (0.000)***	-7.96 (0.000)***
F-ADF test (bcc)	RCP 4.5	75.00 (0.066)*	200.64 (0.000)***	137.29 (0.000)***
	RCP 8.5	87.90 (0.001)***	335.29 (0.000)***	169.44 (0.000)***
F-PP test (bcc)	RCP 4.5	76.51 (0.052)*	201.17 (0.000)***	68.15 (0.000)***
	RCP 8.5	84.15 (0.014)**	575.09 (0.000)***	84.37 (0.014)**
LLC test (Hadley)	RCP 4.5	-16.65 (0.000)***	-9.29 (0.000)***	-6.36 (0.000)***
	RCP 8.5	-17.4 (0.000)***	-17.60 (0.000)***	-8.68 (0.000)***
IPS test (Hadley)	RCP 4.5	-10.03 (0.000)***	-4.48 (0.000)***	-1.94 (0.026)**
	RCP 8.5	-9.27 (0.000)***	-11.77 (0.000)***	-4.23 (0.000)***
F-ADF test (Hadley)	RCP 4.5	311.94 (0.000)***	152.18 (0.000)***	98.28 (0.001)***
	RCP 8.5	322.33 (0.000)***	324.95 (0.000)***	136.08 (0.000)***
F-PP test (Hadley)	RCP 4.5	248.97 (0.000)***	122.66 (0.000)***	126.16 (0.000)***
	RCP 8.5	327.48 (0.000)***	325.57 (0.000)***	149.89 (0.000)***

Note: DF, DPRP and DPET represent the RC of streamflow, precipitation and PET, respectively. P-values are denoted in parentheses. Asterisks represent significance at the 10% (*), 5% (**) and 1% (***) levels.

Table 5
Cointegration test statistics.

Variables	Scenario	Panel ADF	Group ADF	Panel PP	Group PP	Kao (ADF)		
		DF (bcc/Hadley)						
DPRP (bcc)	RCP 4.5	-7.10 (0.000)***	-5.22 (0.000)***	-7.22 (0.000)***	-5.23 (0.000)***	-7.89 (0.000)***		
	RCP 8.5	-3.94 (0.000)***	-2.18 (0.015)***	-3.66 (0.000)***	-1.57 (0.058)*	-9.26 (0.000)***		
DPET (bcc)	RCP 4.5	-6.34 (0.000)***	-4.58 (0.000)***	-5.82 (0.000)***	-4.14 (0.000)***	-9.54 (0.000)***		
	RCP 8.5	-5.54 (0.000)***	-4.17 (0.000)***	-4.35 (0.000)***	-2.76 (0.003)***	-10.20 (0.000)***		
DPRP (Hadley)	RCP 4.5	-19.98 (0.000)***	-30.90 (0.000)***	-19.52 (0.000)***	-28.12 (0.000)***	-1.81 (0.035)**		
	RCP 8.5	-10.22 (0.000)***	-16.48 (0.000)***	-9.19 (0.000)***	-11.50 (0.000)***	-2.06 (0.020)**		
DPET (Hadley)	RCP 4.5	-13.05 (0.000)***	-14.36 (0.000)***	-6.84 (0.000)***	-5.91 (0.000)***	-3.19 (0.001)***		
	RCP 8.5	-11.42 (0.000)***	-11.53 (0.000)***	-12.17 (0.000)***	-13.74 (0.000)***	-1.94 (0.026)**		

Note: DF, DPRP and DPET represent the RC of streamflow, precipitation and PET, respectively. P-values are denoted in parentheses. Asterisks represent significance at the 10% (*), 5% (**) and 1% (***) levels.

the future time period. Uncertainties in the downscaled outputs of GCMs cannot be addressed completely because of its relatively coarse resolution and MACA statistical downscaling methods. Therefore, further research utilizing multiple and ensemble climate projections in the same region is needed. The generalizability of our conclusions may also be improved by considering non-stationarity of LUCC in other study

areas. Further research incorporating additional climate variables and expanded study periods are necessary to fully articulate the relationship between streamflow and climate change.

Table 6Parameter estimation of regression analysis under various climate scenarios.

Scenario	Dependent variable	Independent variables	Coefficient	t-statistic	Probability	R^2
bcc_4.5	DF	Intercept	0.14	3.57	0.000	0.30
		DPRP	1.61	7.66	0.000	
		DPET	-0.11	-2.15	0.032	
bcc_8.5		Intercept	-0.01	-0.33	0.742	0.29
		DPRP	1.28	9.87	0.000	
		DPET	-0.07	-2.51	0.013	
Hadley_4.5		Intercept	0.01	0.39	0.700	0.68
		DPRP	1.52	25.14	0.000	
		DPET	0.04	2.12	0.035	
Hadley_8.5		Intercept	0.14	6.16	0.000	0.74
		DPRP	2.04	29.60	0.000	
		DPET	-0.00	-0.14	0.890	

Note: DF, DPRP and DPET represent the RC of streamflow, precipitation and PET, respectively.

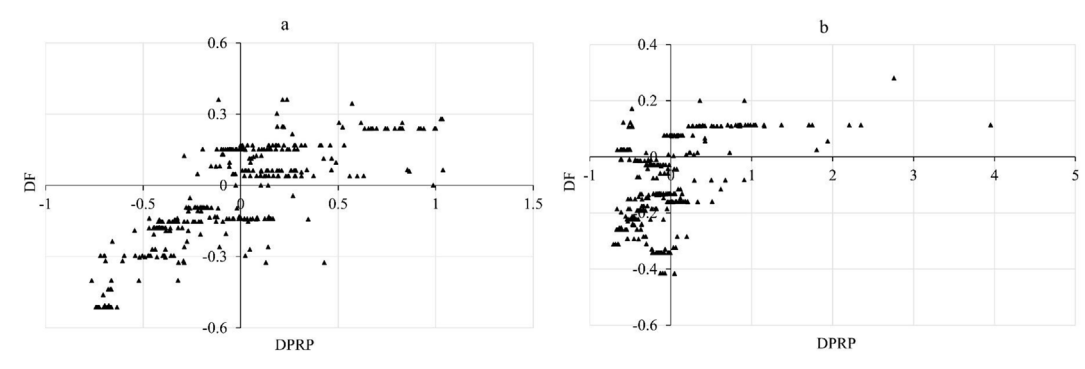


Fig. 7. Distribution of the RCs of precipitation (DPRP) and streamflow (DF) under RCP 4.5 in the Hadley model (a) and bcc model (b). Quadrant numbering proceeds counter-clockwise from the upper right.

CRediT authorship contribution statement

Hui Wang: Conceptualization, Methodology, Investigation, Software, Writing - original draft, Writing - review & editing. **Scott R. Stephenson:** Conceptualization, Supervision, Writing - review & editing. **Shijin Qu:** Software, Formal analysis, Writing - review & editing.

Declaration of Competing Interest

The authors declare that they have no known competing financial interests or personal relationships that could have appeared to influence the work reported in this paper.

Acknowledgements

This publication was made possible by the NSF Idaho EPSCoR Program and by the National Science Foundation under award number OIA-1757324. Its contents are solely the responsibility of the authors and do not necessarily represent the official views of NSF.

References

Abatzoglou, J.T., Brown, T.J., 2012. A comparison of statistical downscaling methods suited for wildfire applications. Int. J. Climatol. 32, 772–780.

Abbaspour, K.C., 2013. SWAT-CUP 2012. SWAT Calibration Uncertainty Program—A User Manual.

Allen, R.G., Pereira, L.S., Raes, D., et al., 1998. Crop evapotranspiration-Guidelines for computing crop water requirements-FAO Irrigation and drainage paper 56, Rome.

Almeida, R.A., Pereira, S.B., Pinto, D.B., 2018. Calibration and validation of the SWAT hydrologic model for the Mucuri River basin. Engenharia Agrícola 38, 55–63.

Arnold, J.G., Srinivasan, R., Muttiah, R.S., et al., 1998. Large area hydrologic modeling and assessment part I: model development 1. JAWRA J. Am. Water Resour. Assoc. 34, 73–89.

Arsanjani, J.J., Helbich, M., Kainz, W., et al., 2013. Integration of logistic regression, Markov chain and cellular automata models to simulate urban expansion. Int. J. Appl. Earth Obs. Geoinf. 21, 265–275.

Aşıcı, A.A., 2013. Economic growth and its impact on environment: a panel data analysis. Ecol. Ind. 24, 324–333.

Bellouin, N., Collins, W., Culverwell, I., et al., 2011. The HadGEM2 family of met office unified model climate configurations. Geosci. Model Dev. 4, 723–757.

Biemans, H., Hutjes, R., Kabat, P., et al., 2009. Effects of precipitation uncertainty on discharge calculations for main river basins. J. Hydrometeorol. 10, 1011–1025.

Borenstein, M., Hedges, L.V., Higgins, J.P., et al., 2010. A basic introduction to fixedeffect and random-effects models for meta-analysis. Res. Synthesis Methods 1, 97–111.

Bronstert, A., Niehoff, D., Bürger, G., 2002. Effects of climate and land-use change on storm runoff generation: present knowledge and modelling capabilities. Hydrol. Processes 16, 509–529.

Can, T., Xiaoling, C., Jianzhong, L., et al., 2015. Assessing impacts of different land use scenarios on water budget of Fuhe River, China using SWAT model. Int. J. Agric. Biol. Eng. 8, 95–109.

Cibin, R., Sudheer, K., Chaubey, I., 2010. Sensitivity and identifiability of stream flow generation parameters of the SWAT model. Hydrol. Processes 24, 1133–1148.

Devia, G.K., Ganasri, B., Dwarakish, G., 2015. A review on hydrologic models. Aquat. Procedia 4, 1001–1007.

Duan, K., Sun, G., McNulty, S.G., et al., 2017. Future shift of the relative roles of precipitation and temperature in controlling annual runoff in the conterminous United States. Hydrol. Earth System Sci. 21, 5517-5529.

Fan, J.-L., Hu, J.-W., Kong, L.-S., et al., 2017. Relationship between energy production and water resource utilization: a panel data analysis of 31 provinces in China. J. Cleaner Prod. 167, 88–96.

Fekete, B.M., Vörösmarty, C.J., Roads, J.O., et al., 2004. Uncertainties in precipitation and their impacts on runoff estimates. J. Clim. 17, 294–304.

Fitzmaurice, G.M., Laird, N.M., Ware, J.H., 2012. Applied Longitudinal Analysis. John Wiley & Sons.

Fuka, D.R., Walter, M.T., MacAlister, C., et al., 2014. Using the Climate Forecast System Reanalysis as weather input data for watershed models. Hydrol. processes 28, 5613–5623.

Gassman, P.W., Reyes, M.R., Green, C.H., et al., 2007. The soil and water assessment tool: historical development, applications, and future research directions. Trans. ASABE 50, 1211–1250.

Golubev, V.S., Lawrimore, J.H., Groisman, P.Y., et al., 2001. Evaporation changes over the contiguous United States and the former USSR: a reassessment. Geophys. Res. Lett. 28, 2665–2668.

Halmy, M.W.A., Gessler, P.E., Hicke, J.A., et al., 2015. Land use/land cover change detection and prediction in the north-western coastal desert of Egypt using Markov-CA. Appl. Geogr. 63, 101–112.

Hanson, R.L., 1991. Evapotranspiration and droughts. US Geological Survey Water-Supply Paper 2375: 99-104.

Hipt, F.Od., Diekkrüger, B., Steup, G., et al., 2019. Modeling the effect of land use and climate change on water resources and soil erosion in a tropical West African catchment (Dano, Burkina Faso) using SHETRAN. Sci. Total Environ. 653, 431–445.

Hovenga, P.A., Wang, D., Medeiros, S.C., et al., 2016. The response of runoff and sediment loading in the Apalachicola River, Florida to climate and land use land cover change. Earth's Future 4, 124–142.

Iacono, M., Levinson, D., El-Geneidy, A., et al., 2015. A Markov chain model of land use change. TeMA J. Land Use, Mobility Environ. 8, 263–276.

Jayakrishnan, R., Srinivasan, R., Santhi, C., et al., 2005. Advances in the application of the SWAT model for water resources management. Hydrol. Processes 19, 749–762.

Kao, C., 1999. Spurious regression and residual-based tests for cointegration in panel data. J. Econ. 90, 1–44.

Karmalkar, A.V., Thibeault, J.M., Bryan, A.M., et al., 2019. Identifying credible and diverse GCMs for regional climate change studies—case study: Northeastern United States. Clim. Change 1–20.

Kundu, S., Khare, D., Mondal, A., 2017. Individual and combined impacts of future climate and land use changes on the water balance. Ecol. Eng. 105, 42–57.

Langbein, W.B., 1949. Annual Runoff in the United States. United States Department of Interior, Washington D.C.

Levin, A., Lin, C.-F., Chu, C.-S.J., 2002. Unit root tests in panel data: asymptotic and finite-sample properties. J. Econ. 108, 1–24.

Massetti, E., Mendelsohn, R., 2011. Estimating Ricardian models with panel data. Climate Change Econ. 2, 301–319.

Change Econ. 2, 301–319.

McCabe, G.J., Wolock, D.M., 2011. Independent effects of temperature and precipitation

on modeled runoff in the conterminous United States. Water Resour. Res. 47.
Moriasi, D.N., Arnold, J.G., Van Liew, M.W., et al., 2007. Model evaluation guidelines for systematic quantification of accuracy in watershed simulations. Trans. ASABE 50, 885–900.

Naudé, W.A., 2004. The effects of policy, institutions and geography on economic growth in Africa: an econometric study based on cross-section and panel data. J. Int. Dev. 16, 821–840

Ouyang, F., Zhu, Y., Fu, G., et al., 2015. Impacts of climate change under CMIP5 RCP scenarios on streamflow in the Huangnizhuang catchment. Stoch. Env. Res. Risk Assess. 29, 1781–1795.

Parr, D., Wang, G., 2014. Hydrologic changes in the US Northeast using the Connecticut River Basin as a case study: Part 1. Modeling and analysis of the past. Global Planet. Change 122, 208–222.

Pedroni, P., 1999. Critical values for cointegration tests in heterogeneous panels with multiple regressors. Oxford Bull. Econ. Stat. 61, 653–670.

Pfister, L., Kwadijk, J., Musy, A., et al., 2004. Climate change, land use change and runoff prediction in the Rhine-Meuse basins. River Res. Appl. 20, 229–241.

Powell, J., Reinhard, S., 2016. Measuring the effects of extreme weather events on yields. Weather Clim. Extremes 12, 69–79.

- Sang, L., Zhang, C., Yang, J., et al., 2011. Simulation of land use spatial pattern of towns and villages based on CA–Markov model. Math. Comput. Modell. 54, 938–943.
- Sintros, T., 2010. Forest and Water Climate Adaptation: A Plan for the Ashuelot River Watershed, New Hampshire. In: Griffith G, Paddock W, Thaler T, et al. (eds). Sagle, ID.
- Skuly, B., Asseng, J., Eggleston, P., et al., 2006. Ashuelot River Corridor Management
- Subedi, P., Subedi, K., Thapa, B., 2013. Application of a hybrid cellular automaton–Markov (CA-Markov) model in land-use change prediction: a case study of Saddle Creek Drainage Basin, Florida. Appl. Ecol. Environ. Sci. 1, 126–132.
- The IPCC AR5. (2014) IPCC, 2014: Climate Change 2014: Synthesis Report. Contribution of Working Groups I, II and III to the Fifth Assessment Report of the Intergovernmental Panel on Climate Change. Geneva, Switzerland: IPCC.
- Thorn, A.M., Wake, C.P., Grimm, C.D., et al., 2017. Development of scenarios for land cover, population density, impervious cover, and conservation in New Hampshire, 2010–2100. Ecol. Soc. 22.
- Uniyal, B., Jha, M.K., Verma, A.K., 2015. Assessing climate change impact on water balance components of a river basin using SWAT model. Water Resour. Manage. 29, 4767–4785.
- Viera, A.J., Garrett, J.M., 2005. Understanding interobserver agreement: the kappa statistic. Fam. Med. 37, 360–363.
- Von Grebmer, K., Bernstein, J., de Waal, A., et al., 2015 2015 Global Hunger Index: armed conflict and the challenge of hunger: Intl Food Policy Res Inst.
- Wang, H., Stephenson, S.R., 2018. Quantifying the impacts of climate change and land use/cover change on runoff in the lower Connecticut River Basin. Hydrol. Processes 32, 1301–1312.
- Wang, H., Stephenson, S.R., Qu, S., 2019. Modeling spatially non-stationary land use/ cover change in the lower Connecticut River Basin by combining geographically weighted logistic regression and the CA-Markov model. Int. J. Geographical

- Information Sci. 1-22.
- Wang, S., Ding, Y., Iqbal, M., 2017. Defining runoff indices and analyzing their relationships with associated precipitation and temperature indices for Upper River Basins in the Northwest Arid Region of China. Water 9, 618.
- Wang, X-j, Zhang, J-y, Shahid, S., et al., 2016. Adaptation to climate change impacts on water demand. Mitig. Adapt. Strat. Glob. Change 21, 81–99.
- Wu, C., Hu, B.X., Huang, G., et al., 2018. Responses of runoff to historical and future climate variability over China. Hydrol. Earth System Sci. 22, 1971–1991.
- Wu, F., 2002. Calibration of stochastic cellular automata: the application to rural-urban land conversions. Int. J. Geographical Information Sci. 16, 795–818.
- Wu, L., Long, T-y, Liu, X., et al., 2012. Impacts of climate and land-use changes on the migration of non-point source nitrogen and phosphorus during rainfall-runoff in the Jialing River Watershed, China. J. Hydrol. 475, 26–41.
- Wu, T., Song, L., Li, W., et al., 2014. An overview of BCC climate system model development and application for climate change studies. J. Meteorol. Res. 28, 34–56.
- Xu, J., Chen, Y., Lu, F., et al., 2011. The nonlinear trend of runoff and its response to climate change in the Aksu River, western China. Int. J. Climatol. 31, 687–695.
- Yang, K., Lu, C., 2018. Evaluation of land-use change effects on runoff and soil erosion of a hilly basin—the Yanhe River in the Chinese Loess Plateau. Land Degrad. Dev. 29, 1211–1221.
- Yang, W., Long, D., Bai, P., 2019. Impacts of future land cover and climate changes on runoff in the mostly afforested river basin in North China. J. Hydrol. 570, 201–219.
- Zankel, M., 2004. A Land Conservation Plan for the Ashuelot River Watershed.
- Zimmerman, J., Lester, A., 2006. Spatial distribution of hydrologic alteration and fragmentation among tributaries of the Connecticut River. The Nature Conservancy, Northampton, MA.
- Zuo, D., Xu, Z., Yao, W., et al., 2016. Assessing the effects of changes in land use and climate on runoff and sediment yields from a watershed in the Loess Plateau of China. Sci. Total Environ. 544, 238–250.